Advanced Electronic Materials

ADVANCED ELECTRONIC MATERIALS Open Access

www.advelectronicmat.de

RESEARCH ARTICLE OPEN ACCESS

Electrical Properties and Interfacial Strain in Thermally Oxidized 4H-SiC MOS Structures Under Different Post-Oxidation Annealing

Fabrizio Roccaforte[1] | Salvatore Ethan Panasci[1] | Valerio Votadoro[1] | Salvatore Di Franco[1] | Marilena Vivona[1] | Simone Milazzo[1] | Marco Zignale[1] | Filippo Giannazzo[1] | Béla Pécz[2] | Patrick Fiorenza[1]

[1]Consiglio Nazionale delle Ricerche – Istituto di Microelettronica e Microsistemi (CNR-IMM), Catania, Italy | [2]HUN-REN Centre for Energy Research, Institute of Technical Physics and Materials Science, Budapest, Hungary

Correspondence: Fabrizio Roccaforte (fabrizio.roccaforte@cnr.it)

Received: 17 April 2026 | **Revised:** 7 August 2026 | **Accepted:** 20 August 2026

Keywords: MOSFET | oxidation | silicon carbide | silicon oxide

ABSTRACT

The electrical behavior of SiO_2/4H-SiC interfaces is a central challenge for the development of high-efficiency MOSFETs, where trap states and interfacial structural distortions can affect carrier mobility and device reliability. In this work, we investigate thermally grown SiO_2 on n-type 4H-SiC epilayers, analyzing the effects of different post-oxidation annealings (POAs) in N_2 and Ar on both the electrical response and the interfacial strain. MOS capacitors subjected to POA in N_2 exhibit a marked reduction of interface states density (D_{it}) near the conduction band edge, together with an increase of the electron Fowler–Nordheim barrier height. These electrical signatures occur simultaneously with negative flat-band voltage shifts, suggesting the presence of an interfacial dipole rather than the presence of fixed charges only. Raman spectroscopy reveals that N_2-based POA induces an increase of biaxial tensile strain at the SiO_2/SiC interface, which is less pronounced in the case of POA in Ar. The observation of strain evolution and electrical properties demonstrates that nitrogen incorporation not only passivates dangling bonds but also modifies the interfacial stress state, thereby influencing barrier properties and charge distribution. These findings provide new insights to be considered in the optimization of SiO_2/SiC gate stacks in 4H-SiC MOSFETs.

1 | Introduction

One of the keys for the success of silicon carbide (4H-SiC) over the other wide bandgap semiconductors is the possibility to form silicon dioxide (SiO_2) by thermal oxidation [1]. This processing step is very important in SiC device technology. In fact, thermal oxidation followed by post-oxidation-annealing can be used for the gate insulator in metal oxide semiconductor field effect transistors (4H-SiC MOSFETs) [2], adopted as a sacrificial process to remove surface defects, or to optimize the carrier lifetime by carbon interstitials injection [3]. Consequently, thermal oxidation of SiC has been extensively studied over the years, considering the impact of several parameters, like oxidation temperature and time, substrate doping and orientation [4–6].

The performances of 4H-SiC MOSFETs are largely determined by the properties of the SiO_2/4H-SiC interface established during fabrication [2, 7]. Device parameters such as field effect channel mobility (μ_{FE}) and specific on-resistance (R_{ON}) [8, 9] are typically improved by applying post-oxidation annealing (POA) or post-deposition annealing (PDA) treatments of the SiO_2 gate dielectric in a nitric oxide (NO) or nitrous oxide (N_2O) ambient in a temperature range of 1100°C–1300°C [10]. Nitrogen incorporation during POA/PDA is known to enhance carrier mobility by passivating dangling bonds and, consequently, reducing the density of interface states D_{it}. It has been observed that nitrogen binds directly to SiC, or it gets incorporated within the first atomic layers of the crystal [11], where it can also lead to "counter doping" effects [12, 13] contributing to the mobility improvement.

However, nitridation annealing (either in NO or N_2O) induces a re-oxidation of the interface, which can introduce additional trapping centers at the SiO_2/4H-SiC interface, potentially compromising the stability of the threshold voltage (V_{th}) [14, 15]. Moreover, charge traps located in the oxide layer and in regions close to the interface influence the conduction behavior of n-channel MOSFETs [16].

For that reason, alternative "non-oxidizing" processes have been explored in literature to avoid the formation of interface carbon-related defects, including annealing in a low O_2 partial pressure [17], engineered nitridation of the surface [18, 19], low temperature silicon films oxidation [20] H_2-based interface preparation treatments before SiO_2 and N_2 annealing [21] or alternative wide bandgap oxides configurations of the gate stack [22].

The negative flat band voltage (V_{FB}) shift observed under certain POA conditions in NO has been attributed to a dipole layer generated by the formation of stable Si—N bonds at the interface during POA [23]. In this context, efficient passivation of interface states can be achieved also by N_2 annealing in low O_2 partial pressure [24], and the presence of oxygen during low temperature POA removes the nitridation drawbacks, while preserving the nitrogen at the interface [25].

In these works, a remaining open question is whether the D_{it} reduction and μ_{FE} improvement are only due to the saturation of dangling bonds and counter doping, or if other structural modifications of the SiC crystal are induced by POA or PDA processes.

Other works speculated that strain/stress at SiO_2/SiC interface induced during the gate oxide formation SiC can be critical for understanding the device behavior. In fact, it has been shown that thermal oxidation can lead to compressive strain in the oxide and lead to interface defects [26]. As an alternative to conventional nitridation, the introduction of foreign species (e.g. B, Ba, Sr, etc.) at the SiO_2/SiC interface has been proposed to improve 4H-SiC MOSFET mobility [27, 28]. In the case of B, a structural change in SiO_2 near the interface caused by stress relaxation has been invoked as the driving force for D_{it} reduction, rather than a termination of dangling bonds [27]. Instead, a strain relaxation of the underlying SiC has been demonstrated in the case of the introduction of alkali and alkaline-earth elements at the SiO_2/SiC interface [29].

Although all these mechanisms have been extensively investigated individually, a direct experimental correlation between interfacial strain and electrical properties of thermally oxidized SiO_2/4H-SiC interfaces has not yet been established. In particular, it remains unclear whether the modifications induced by POA originate solely from chemical passivation of interface defects or also involve strain-driven charge redistribution capable of modifying the electrostatic potential at the interface. Establishing such a correlation is essential for understanding the simultaneous evolution of interface-state density, flat-band voltage and Fowler–Nordheim barrier height.

In this paper, we report on the electrical properties of thermally oxidized 4H-SiC MOS structures under different POA atmospheres, combining electrical characterization (C–V, I–V and Fowler–Nordheim analysis) with depth-resolved Raman spectroscopy. Rather than focusing solely on interface states passivation, we demonstrate that the evolution of the electrical characteristics is accompanied by relevant modifications of the interfacial strain. By correlating the Raman-derived strain and electrical parameters, we show that the observed increase of the Fowler–Nordheim barrier height together with the negative flat-band voltage shift is consistent with the formation of an interfacial dipole associated with both chemical bonding and strain-induced charge redistribution. These findings provide a broader physical framework for engineering SiO_2/SiC gate stacks beyond conventional interface passivation.

2 | Results and Discussion

While the thermal oxidation of SiC has been extensively studied in literature, considering the impact of several parameters, like oxidation temperature and time, substrate doping and orientation [4–6], most of the reported works refer to highly doped substrates. Hence, to precisely define our baseline process, we have first studied the oxidation kinetics directly on the n-type doped epilayers used for our MOS fabrication.

Figure 1a displays a representative AFM scan acquired on lithographic patterns to determine the oxide thickness after thermal annealing in O_2 at 1100°C for 2 h. A step height of ~15 nm has been measured between SiO_2 covered and bare 4H-SiC. Cross-sectional TEM in Figure 1b provided a further confirmation of the grown SiO_2 thickness. Hence. this validated AFM-based methodology has been repeated to determine the oxide thickness for all the oxidation conditions at different temperatures and times.

Figure 2a shows the thermal oxide thickness as a function of the oxidation time, for three different temperatures (1100°C, 1150°C, and 1200°C). As can be seen, the oxide thickness increases with increasing the oxidation temperature and time, following a clear trend.

A modified Deal–Grove model, based on the established Si oxidation process, has been often invoked to describe SiC oxidation kinetics [4]. Accordingly, the oxide thickness x is given by

$$x^2 + Ax = B(t + \tau) \quad (1)$$

where t is oxidation time, τ is related to an initial oxide thickness, B and B/A are parabolic and linear kinetic constants, respectively [4]. B/A is related to the surface reaction of oxygen with SiC, while B is associated to the in-diffusion of oxidizing species through the oxide. Evidently, the experimental data were described by this model, as shown by the fits reported in Figure 2a. Figure 2b,c depicts the Arrhenius plots of the linear (B/A) and parabolic (B) rate constants, determined by the Deal-Grove model.

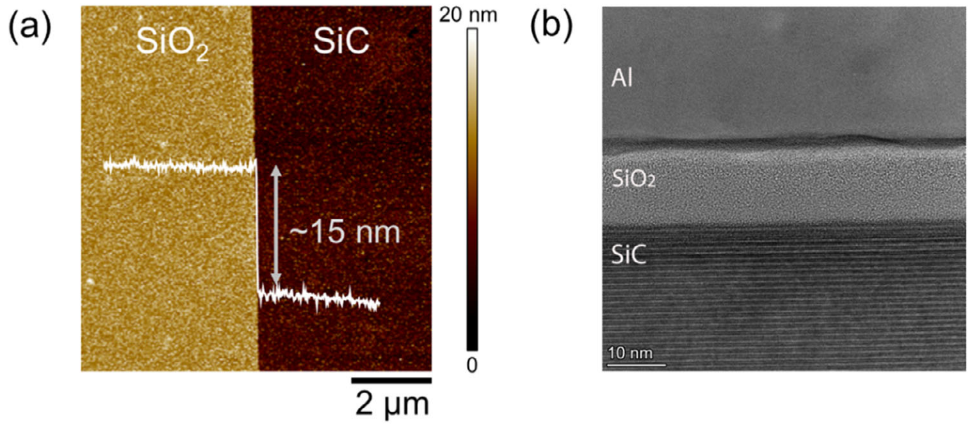

FIGURE 1 | (a) AFM scan of the SiO_2 step height on 4H-SiC showing a thickness of ~15 nm. (b) Cross-sectional TEM image of the SiO_2/4H-SiC interface, confirming the thickness of the thermally grown SiO_2. The images are representing the case of the oxide formed at 1100°C in O_2 for 2 h.

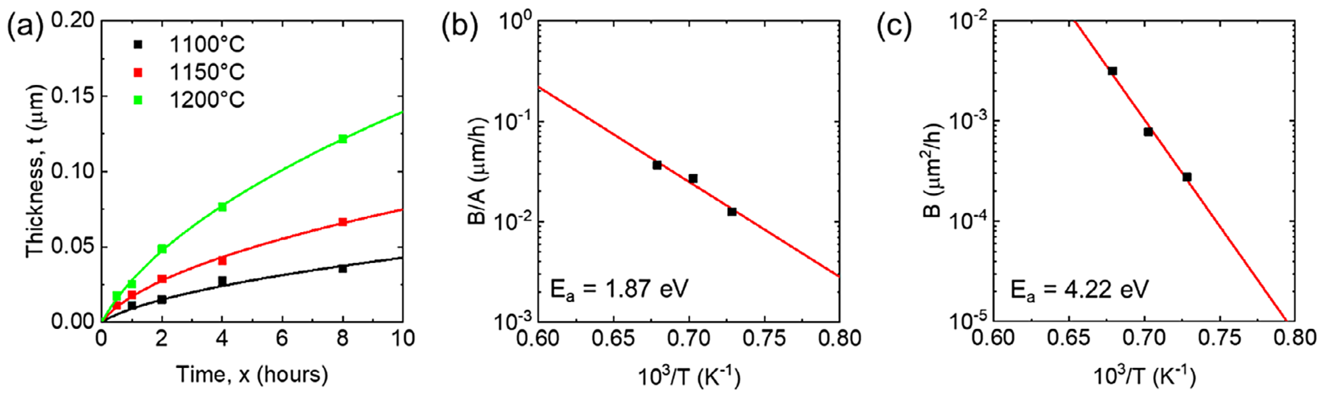

FIGURE 2 | (a) Thermal oxide thickness as a function of the oxidation time for three different temperatures: 1100°C, 1150°C, and 1200°C. Arrhenius plot of B/A as a function of the inverse of temperature in the linear (b) and in (c) the parabolic region. The activation energies are also reported.

The activation energies found by the linear fit in a semilog scale were 1.87 and 4.22 eV, for the linear and parabolic oxidation regime, respectively. These values are higher than those reported by other authors for similar doping level [4, 5]. This result confirms that the oxidation kinetics depends strongly on the experimental annealing conditions, surface preparation and material quality.

Then, for the electrical characterization of the oxides, MOS capacitors have been fabricated on epitaxial samples, following the sequences schematically reported in Figure 3a. First, the 4H-SiC epitaxial samples have been cleaned in acetone and isopropanol, followed by a piranha etch in H_2SO_4:H_2O_2 = 3:1 for 10 min at 100°C, and an immersion in diluted hydrofluoric acid HF:H_2O = 1:5 for 10 min at room temperature. Then, thermal oxidation has been carried out at 1150°C for 2 h in O_2, followed by appropriate post-oxidation annealing (POA) in N_2 (1150°C or 1200°C) or Ar (1150°C) for 2 h. After selective removal of the oxide formed on the sample back-side, e-beam evaporation of 200nm thick Al films has been carried out on both the front and back-side of the samples. Photolithography and Al wet etch were employed to define the front electrodes of the MOS capacitors of different area (see optical microscopy image in Figure 3b.

Then C-V measurements have been performed at 1kHz on the MOS capacitors to get insights into the properties of the thermally grown oxide and on the effect of the POA.

Figure 4a shows the C-V curves collected on the thermal oxide (as oxidized) and on the same oxide subjected to different POA processes at 1150°C in N_2 for 2 h (N2_1150), 1200°C in N_2 for 2 h (N2_1200) and 1150°C in Ar for 2 h (Ar_1150). The curves clearly indicate that while the as oxidized sample exhibits an experimental flat-band voltage V_{FB}^{exp} close to the ideal value V_{FB}^{ideal} (dashed line), POA of the samples induces a negative shift independently of the annealing atmosphere. The V_{FB}^{ideal}= 0.98 eV has been determined considering the Al work function (4.28 eV), the 4H-SiC electron affinity (3.1 eV) and the epilayer donor concentration ($N_D = 1 \times 10^{16} cm^{-3}$) [30].

Such a negative shift is often associated to the presence of a positive fixed charge N_F given by:

$$N_F = \frac{C_{ox}}{q}\left(V_{FB}{}^{ideal} - V_{FB}{}^{exp}\right) \quad (2)$$

where C_{ox} is the accumulation capacitance, q is the electron charge.

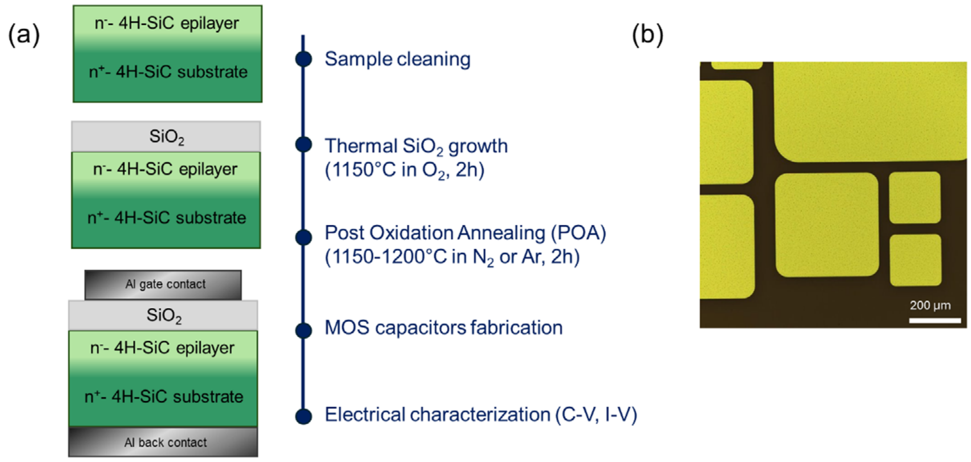

FIGURE 3 | (a) Schematic fabrication flow-chart of the MOS capacitors, from sample cleaning to thermal oxidation up to the final electrical characterization. (b) Optical microscopy image of the fabricated Al/SiO_2/4H-SiC MOS capacitors.

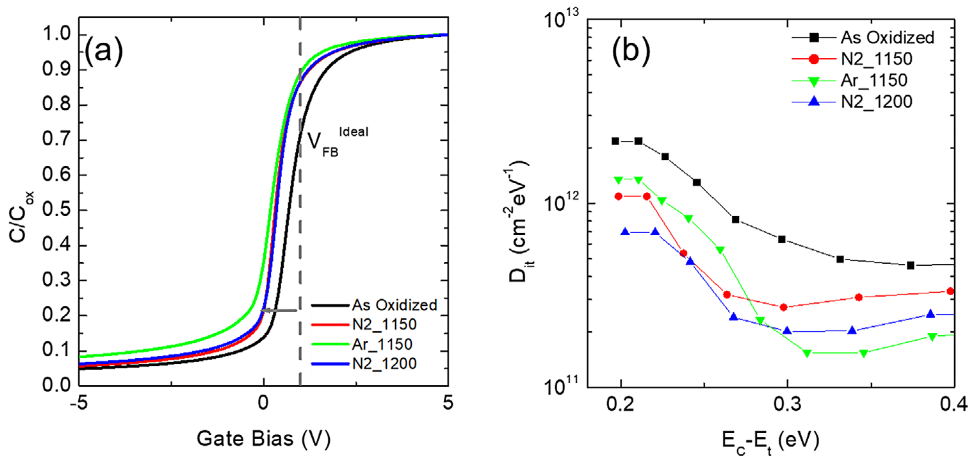

FIGURE 4 | (a) C-V curves collected on the thermally grown SiO_2 (as oxidized) and on the samples subjected to subsequent POA at 1150°C in N_2 for 2 h (N2_1150), 1200°C in N_2 for 2 h (N2_1200) and 1150°C in Ar for 2 h (Ar_1150). The dashed line indicates the position of the ideal flat band voltage. (b) Interface states density (D_{it}) of the same samples determined from the previous C-V curves using the Terman's method. The decrease of the interface states density below the conduction band edge upon POA is clearly visible.

The values of N_F determined by Equation (2) are in the range 5–6 $\times$ 10^{11}cm^{-2}. This experimental finding suggests that the negative flat-band voltage shift is not related only to the nitrogen incorporation at the interface, since the Ar_1150 sample presents a similar behavior.

Moreover, from these C-V curves, by applying the modified Terman's method proposed by *Zignale* et al. [31], which compares the experimental low frequency (1kHz) curve with the theoretical C-V curve, it was possible to determine the interface trap density D_{it} energy profiles (reported in Figure 4b). As can be noticed, the POA in Ar produced a reduction of the D_{it} from 2.5×10^{12} cm^{-2}eV^{-1} (as oxidized) down to 1.5×10^{12} cm^{-2}eV^{-1} (Ar_1150), most probably due to a partial reorganization of the interface owing to the provided thermal budget. Moreover, it is known that Ar annealing can induce the decomposition and ejection of carbon byproducts formed during thermal oxidation [32], thus also explaining the observed D_{it} reduction even in a neutral annealing ambient. On the other hand, the D_{it} reduction is more pronounced in the case POA in N_2, where the incorporation of nitrogen can lead to the passivation of dangling bonds by to the formation of Si—N bonds, reaching a minimum of $D_{it} = 7 \times 10^{11}$ cm^{-2}eV^{-1}, at 0.2 eV from the bottom of the conduction band, after the process in N_2 at 1200°C.

Figure 5a shows the gate current vs oxide electric field curves, collected on the as oxidized sample and on the samples subjected to POA. It can be noticed that the as oxidized sample shows an onset of the gate current at lower gate bias values compared to the samples subjected to POA. This experimental evidence suggests that a variation of the energy barrier height to the electron tunnelling occurs after POA. In addition, it is interesting to note that the as oxidized sample and the samples subjected to POA in N_2 present similar current slopes in semi-log scale, while the sample subjected to POA in Ar exhibits a reduced slope. The estimated breakdown field also increased after POA in N_2

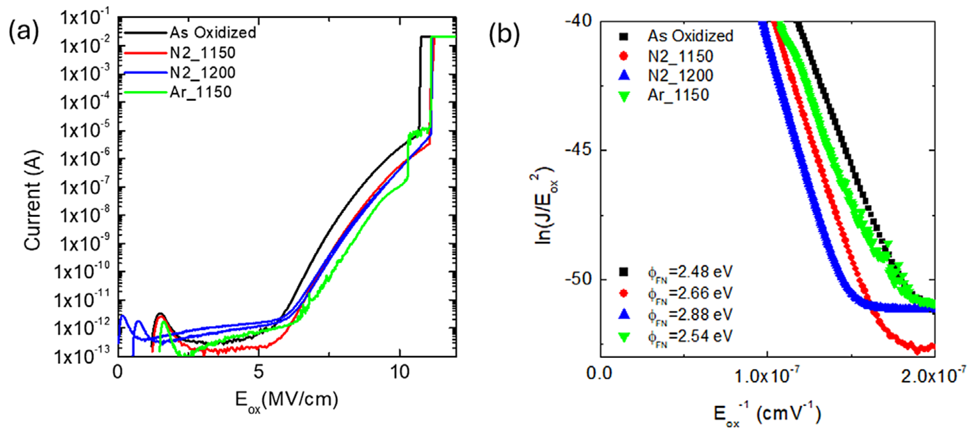

FIGURE 5 | (a) Gate current versus oxide electric field E_{ox} plots for the as oxidized sample and for the samples subjected to different POA conditions: 1150°C in N_2 for 2 h (N2_1150), 1200°C in N_2 for 2 h (N2_1200) and 1150°C in Ar for 2 h (Ar_1150). (b) Logarithmic plot of the current density divided by the square of the oxide electric field ($\ln J/E_{ox}^2$) as a function of the reverse oxide electric field (E_{ox}^{-1}). From these curves the Fowler-Nordheim barrier height has been determined for the different cases, using Equations (3) and (4).

(11.1 MV/cm) compared to the as oxidized (10.7 MV/cm) and Ar_1150 samples (10.1 MV/cm).

To get insights on this aspect, the Fowler-Nordheim (FN) plots were quantitatively analyzed (Figure 5b). In particular, the FN tunnelling current density J_{FN} is related to the electric field across the oxide E_{ox} by:

$$J_{FN} = AE_{ox}^2 exp\left(-\frac{B}{E_{ox}}\right) \tag{3}$$

Where:

$$A = \frac{q^3\left(\frac{m}{m_{ox}}\right)}{8\pi h\Phi_{FN}} \tag{4}$$

$$B = \frac{8\pi\sqrt{2m_{ox}\Phi_{FN}^3}}{3qh} \tag{5}$$

Here, m and m_{ox} are the free and effective electron masses, respectively, and q is the electron charge, h is the Plank constant, and Φ_{FN} is the tunneling barrier height for electrons [33].

Since the presence of an effective charge in the oxide can act as an electrostatic screen affecting the FN barrier height, the electric field E_{ox} in the FN plots has been calculated considering the experimental flat band voltage shift:

$$E_{ox} = \frac{\left(V_G - V_{FB}^{exp}\right)}{t_{ox}} \tag{6}$$

Figure 5b reports the FN plots, i.e. the logarithmic plot of the current density divided by the square of the oxide electric field as a function of the reverse oxide electric field. By the fit of the experimental curves with Equation 3, it was possible to extract the values of Φ_{FN} for the different cases. As can be noticed, while the as oxidized sample has a barrier of 2.48 eV, the values of Φ_{FN} increased after POA in N_2 (N2_1200) up to 2.88 eV, thus suggesting the presence of a negative charge that enhances the barrier height to the electrons' tunneling. However, the C-V curves (Figure 4a) clearly showed a negative shift of the C-V curves with respect to the theoretical one, which is inconsistent with the experimentally observed increase of the barrier height. Similarly, the Ar_1150 sample also showed a higher barrier Φ_{FN} (2.54eV) compared to the as oxidized, but lower than the N2_1200 sample (2.88eV). Then, independent of the POA, the electrical behaviour of the MOS cannot be uniquely attributed to the presence of fixed charges in the oxide.

It must be pointed out that other transport mechanisms like trap assisted tunnelling (TAT), Schottky emission or Poole–Frenkel emission cannot explain our experimental data, either due to the large oxide thickness or to the weak experimental temperature coefficient of the barrier height [34].

Raman spectroscopy was employed to provide a deeper explanation of the electrical behavior of the MOS capacitors, as it represents a valid and non-invasive technique employed for the evaluation of crystalline quality, strain and doping effects on silicon carbide [35].

Figure 6a,b report the representative Raman peaks of 4H-SiC n-epilayer (~10^{16} cm^{-3}) grown on a highly doped n^+ substrate of ~10^{19} cm^{-3}. More specifically, the main Raman features are the optical transverse *in-plane* mode (E_2(TO) and the optical longitudinal *out-of-plane* (A_1(LO)), visible in Figure 6a,b. These two vibrational modes are very sensitive to strain effects on SiC [36, 37]. Specifically, their red- and blue-shift correspond to tensile and compressive strain, respectively, as indicated by the arrows in Figure 6a,b.

To demonstrate that these features are sensitive to the SiC side of the SiO_2/SiC interface, we carried out a spectroscopic analysis at different depths, as indicated by the scheme of Figure 6c, for the as oxidized sample (1150°C in O_2 for 2 h). By setting the focus on the sample surface (Z = 0), the E_2(TO) peak is centred at ~776.40 cm^{-1}. When the focus is moved deeper in the sample (from 2 to 6 μm), the E_2(TO) peak undergoes a blue-shift to ~776.55 cm^{-1}, i.e.

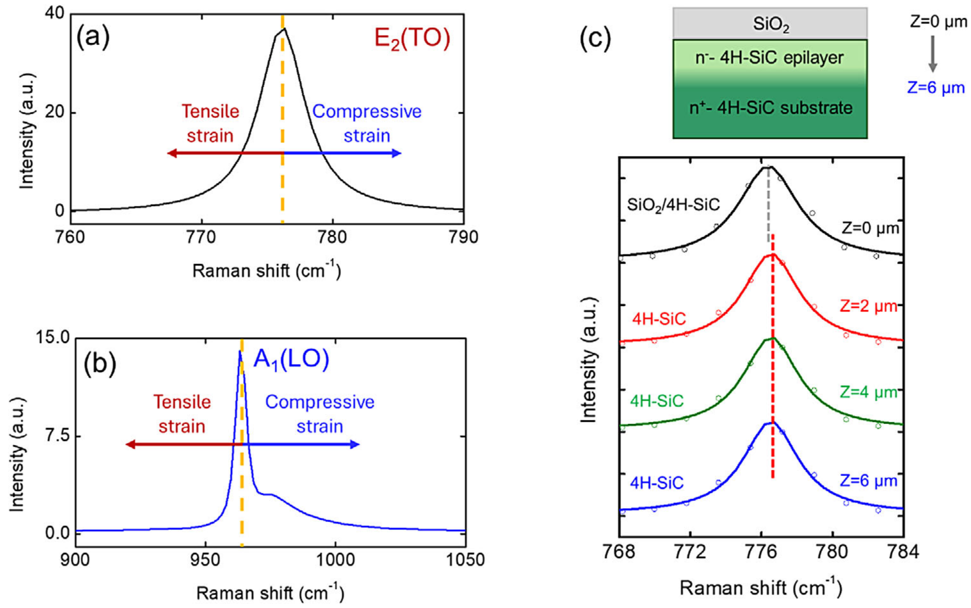

FIGURE 6 | Representative Raman spectrum of 4H-SiC acquired by a laser wavelength excitation of 532 nm, with detail on (a) the transverse optical in-plane mode (E_2) and (b) the longitudinal optical A_1(LO). The red and blue arrows indicate the direction of the peaks when subjected to tensile and compressive strain, respectively. (c) Scheme of the SiO_2/4H-SiC samples and the corresponding E_2 (TO) peaks acquired at different depths (from 0 to 6 μm).

closer to the E_2(TO) of the unstrained 4H-SiC. This latter indicates that the method is sensitive to the strain variation at the SiO_2/SiC interface.

To evaluate the strain effects on 4H-SiC induced by thermal oxidation and subsequent POA, several Raman maps have been carried out on areas of 40 × 40 μm^2, collecting more than 6000 spectra for each sample. Here, it is important to underline that the longitudinal modes can be also dependent on doping effects, but only at high doping levels (e.g. 10^{17}–10^{19} cm^{-3}) [38]. Hence, in our samples ($N_D = 1 \times 10^{16} cm^{-3}$) any shift of the Raman modes can be attributed to strain variations.

A statistical analysis was carried out on the different samples by fitting with Gaussian functions the main peaks for all the Raman spectra. From the distributions of the E_2(TO) and A_1(LO) peaks positions, the mean values and the standard deviation of the two contributions have been extrapolated. This evaluation is reported in Figure 7a,b, where we considered the starting 4H-SiC (before treatments) as the reference condition of "unstrained" sample, showing E_2 and A_1 peaks centered at 776.55 ± 0.05 cm^{-1} and 964.40 ± 0.07 cm^{-1}, respectively. A dashed line ("reference line") serves as guide for the eye to identify the unstrained condition in Figure 7a,b. After thermal oxidation at 1150°C in O_2 for 2 h (white area), both the E_2 and A_1 modes displayed a red-shift, indicating a tensile strain effect induced by the growth of the SiO_2 film on the top of 4H-SiC surface. To strengthen this hypothesis, a thermal annealing in Ar atmosphere on the starting 4H-SiC reference sample was carried out at 1150°C for 2 h (4H-SiC_Ar). As can be seen, the two vibrational modes observed under this annealing condition are almost unchanged with respect to the reference line. This result confirms that the strain is a consequence of the oxidation and not of the thermal budget.

Then, the as oxidized samples were subjected to POA either in Ar (Ar_1150) or in N_2 (N2_1150 and N2_1200). The POA in Ar at 1150°C for 2 h showed an E_2 peak position comparable with the reference line, and an A1 peak position close to the as oxidized sample. Differently, the POAs in N_2 (N2_1150 and N2_1200) induced higher E_2 and A_1 peaks variations (higher tensile strain) compared to the untreated and to the as oxidized samples.

As proposed by *Zhang* et al. [37], a quantification of the stress on the samples is possible by comparing the Raman peaks of the reference 4H-SiC (unstrained) with those of the oxidized and annealed samples. In particular, the as-oxidized sample displayed a stress of ~29 MPa, close to the value determined for the POA in Ar (~24 MPa). On the other hand, the POAs in N_2 showed a significantly higher stress of ~109 and ~112 MPa for N2_1150 and N2_1200, respectively.

The scenario emerging from the previously shown experimental results can be summarized in Figure 8. This graph highlights a systematic association between the stress obtained by Raman analysis and the interface-state density across the investigated processing conditions (As oxidized, Ar_1150, N2_1150 and N2_1200). After thermal oxidation of 4H-SiC, a high density of interface states D_{it} near the conduction band edge (2.5 × 10^{12} $cm^{-2}eV^{-1}$) is derived by C-V analysis, thus being typically attributed to the formation of a defective non-stoichiometric interface [39]. At the same time, a tensile strain is induced by the oxidation process, as revealed by Raman spectroscopy and illustrated in Figure 8b,c. After POA, a reduction of D_{it} occurs, due to a reorganization of the interface, being this D_{it} reduction more significant after POA in N_2 (7 × 10^{11} $cm^{-2}eV^{-1}$) than in Ar (1.5 × 10^{12} $cm^{-2}eV^{-1}$), due to a chemical passivation of the dangling bonds in nitrogen atmosphere. Concurrently, the

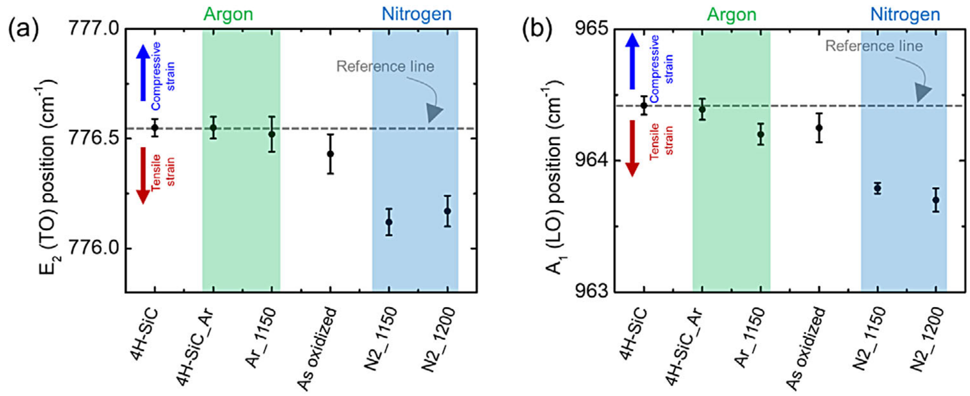

FIGURE 7 | Raman peaks positions E_2 (TO) (a) and A_1(LO) (b) for the different samples (from left to right): 4H-SiC reference (4H-SiC), thermal treatment in Ar atmosphere at 1150°C for 2 h (4H-SiC_Ar), after thermal oxidation and subsequent POA in Ar at 1150°C for 2 h (Ar_1150), after thermal oxidation (as oxidized), after thermal oxidation and subsequent POA in N_2 environment at 1150°C for 2 h (N2_1150) and after thermal oxidation and subsequent POA in N_2 at 1200°C for 2 h (N2_1200). The trend shown by the Raman peaks indicates an effect of the POA on the interfacial strain.

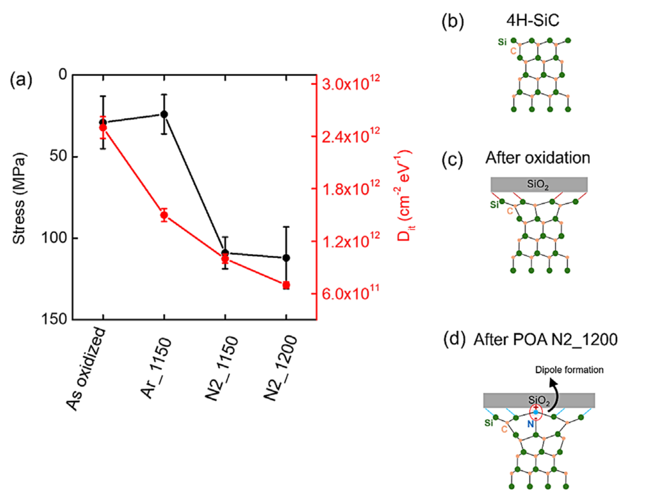

FIGURE 8 | (a) Stress (MPa) and interface state density D_{it} (at 0.2 eV from the bottom of the conduction band) for the four samples considered in this paper (As oxidized, Ar_1150, N2_1150, N2_1200). Schematic illustration of the system before oxidation (b), after oxidation (c) and after POA in N2_1200 (d).

near-surface atoms of 4H-SiC are forced to stretch outward (increase in tensile strain) to mechanically accommodate the contraction induced by incorporation of nitrogen, as illustrated in Figure 8d.

Clearly, establishing a quantitative correlation between interface state density and stress would require more systematic experiments for the acquisition of a large number of data, which is out of the scope of this paper. Nevertheless, our results preliminarily demonstrate that near-interface lattice modifications must be considered for a complete description of the SiO_2/SiC system subjected to nitrogen-based annealings.

The C-V curves of the samples subjected to POA in N_2 or Ar exhibit a negative flat-band voltage shift with respect to the ideal value, suggesting the presence of a net positive fixed charge in the system in the order of $5–6 \times 10^{11} cm^{-2}$. However, at the same time an increase of the electron Fowler–Nordheim barrier heights are found by the I-V analyses, which would be consistent with the presence of a negative charge. Clearly, this unexpected electrical behavior cannot be uniquely attributed to the presence of fixed charges in the oxide.

Hence, as previously hypothesized for other systems [40–42], also in our case the presence of an interfacial dipole must be invoked to explain the experimental results. Such a dipole arises from the interfacial lattice deformation and charge redistribution occurring after POA and is stronger in the case of POA in N_2 due to the chemical nature of the Si—N bond.

As a matter of fact, Raman spectroscopy reveals that nitrogen-based POA exhibits a more pronounced increase of both in-plane and out-of-plane tensile strain at the SiO_2/SiC interface respect to the POA in Ar, due to the presence of chemically reactive species.

This scenario is schematically illustrated in Figure 9, showing the MOS band diagram without (Figure 9a) and with (Figure 9b) an interfacial dipole.

Recent theoretical investigations have clarified that two distinct dipole contributions can coexist at the SiO_2/SiC interface: an intrinsic dipole associated with the abrupt oxide/semiconductor transition and structural rearrangements, and an additional extrinsic dipole induced by nitrogen incorporation [43]. In this framework, the dipole observed after Ar POA can be ascribed primarily to the intrinsic component, originating from interfacial bonding asymmetry and strain-induced charge redistribution in the absence of foreign species.

Conversely, in the case of N_2 POA, the formation of Si—N bonds introduce an additional, chemically-driven dipole due to the higher electronegativity of nitrogen, leading to a more pronounced charge separation at the interface. The combined effect of intrinsic and nitrogen-induced dipoles provides a consistent explanation for the larger increase in the Fowler–Nordheim barrier height observed after N_2 annealing, with the magnitude of this effect being further enhanced by the higher tensile strain revealed by Raman analysis.

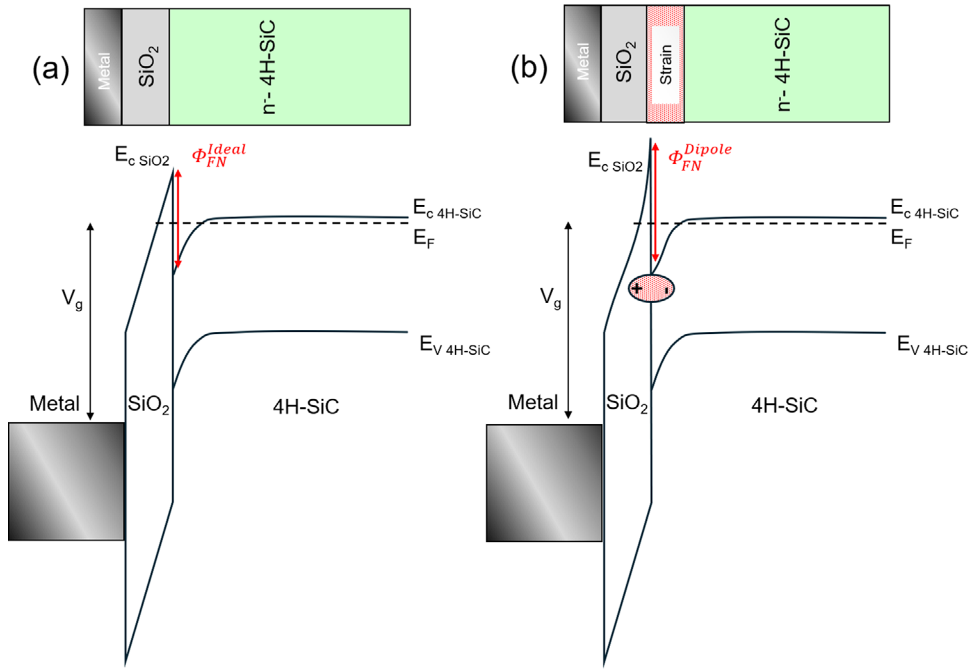

FIGURE 9 | Schematic MOS interface band diagram without (a) and with (b) an interfacial dipole that increases the FN electron barrier height. The upper part of the figure schematically shows the MOS structures (not in scale).

Kil et al. [23] estimated a dipole charge density in the order of 1×10^{14} cm^2 after PDA in NO, which is consistent with the typical density of nitrogen atoms revealed in NO-nitridated SiO_2/SiC interfaces. However, in our case, the different POA atmosphere (N_2) and annealing temperature (1200°C) suggest a lower interfacial nitrogen incorporation and, hence, less pronounced dipole effect.

3 | Conclusion

In this work, the impact of different post-oxidation annealings of thermal oxide on both the electrical behavior and the interfacial strain of SiO_2/4H-SiC MOS structures has been studied.

Nitrogen annealing in N_2 at 1150°C–1200°C reduces the interface states density and increases the Fowler–Nordheim tunneling barrier height, confirming the beneficial role of nitrogen incorporation toward interface passivation. The simultaneous negative V_{FB} shift, and barrier height increase can be explained by invoking the formation of an interfacial dipole layer, rather than a simple variation of fixed charges. In fact, Raman spectroscopy revealed that these electrical improvements are associated with an increase in tensile strain at the SiO_2/SiC interface, after POA in N_2. In contrast, Ar annealing has a lower impact on the strain and on electrical parameters.

Hence, the main outcome of this work is that N_2-based POA simultaneously modifies the chemical bonding, the interfacial strain and the electrostatic potential of the SiO_2/4H-SiC interface. The experimental correlation found between strain and electrical parameters suggests that strain-induced charge redistribution contributes to the formation of an interfacial dipole, providing a broader physical framework for understanding the electrical behavior of SiC MOS interfaces beyond conventional defect passivation.

4 | Experimental Section/Methods

N-type 4H-SiC (0001) epilayers with a doping concentration of $N_D = 1 \times 10^{16} cm^{-3}$, grown onto highly doped substrates were used in these experiments. Thermal oxidation in "dry" O_2 at atmospheric pressure was studied in the temperature range 1100°C–1200°C. After the oxidation process, the grown oxide thickness, determined by measuring the step height of lithographic patterns, was measured employing a Bruker Icon Dimension system for Atomic Force Microscopy (AFM) imaging in tapping mode (silicon tips with a nominal curvature radius of 10 nm and a frequency of 300 kHz). On selected samples, a more accurate inspection of the oxide thickness and the SiO_2/SiC interface flatness has been carried out by Transmission Electron Microscopy (TEM), employing an aberration-corrected Titan Themis 200 microscope by Thermo Fisher for high-resolution transmission electron microscopy (HR-TEM). Then, metal oxide semiconductor (MOS) capacitors have been fabricated defining Al contacts on the oxide and a large area back contact on the sample rear. More details on MOS capacitors' fabrications are reported in the text. The MOS capacitors were then electrically characterized by capacitance-voltage (C-V) and current-voltage (I-V) measurements performed to assess the SiO_2/SiC interface electrical properties using a Keysight B1500A Parameter Analyzer connect to an MPI TS200 HP probe station. Different POA conditions were employed before the formation of metal electrodes and electrical characterizations. All the oxidation and post-oxidation annealing were carried out in an atmospheric pressure Expertech CTR-200 horizontal furnace. A set of 10 MOS capacitors has been measured for each annealing condition. The reported results are representative of the average behavior observed in the different annealing conditions. Finally, the strain induced by thermal oxidation processes was estimated by Raman spectroscopy characterization using a Renishaw inVia confocal microscope with an excitation laser wavelength of 532 nm combined with a 100× objective, and a grating of 1800 l/mm.

Acknowledgements

The authors would like to thank G. Greco, R. Lo Nigro and E. Schilirò (CNR-IMM) for technical support and scientific discussion on the oxidation kinetics. This work was partially carried out in the framework of the MicroTech_for_Green project, funded by Ministero delle Imprese e del Made in Italy (MIMIT) under IPCEI Microelettronica 2, using the facilities of the Italian Infrastructure Beyond-Nano. Moreover, the authors acknowledge the Wide Bandgap (WBG) Pilot Line, funded jointly by the Chips JU, through the European Union's Digital Europe programme and Horizon Europe programme, as well as by the participating states Italy, Sweden, Poland, Finland, Austria, France and Germany, under Grant Agreement n. 101183211. Funding for travels from CNR/HAS (2023-2025) bilateral project GHOST-III is also acknowledged.

Open access publishing facilitated by Consiglio Nazionale delle Ricerche, as part of the Wiley - CRUI-CARE agreement.

Conflicts of Interest

The authors declare no conflicts of interest.

Data Availability Statement

The data that support the findings of this study are available from the corresponding author upon reasonable request.

References

1. T. Kimoto and J. A. Cooper, *Fundamentals of Silicon Carbide Technology: Growth, Characterization, Devices, and Applications*, 1st Edition (John Wiley & Sons Singapore Pte. Ltd, 2014).

2. F. Roccaforte, P. Fiorenza, G. Greco, et al., "Emerging Trends in Wide Band Gap Semiconductors (SiC and GaN) Technology for Power Devices," *Microelectronic Engineering* 187 (2018): 66–77.

3. T. Hiyoshi and T. Kimoto, "Reduction of Deep Levels and Improvement of Carrier Lifetime in n-Type 4H-SiC by Thermal Oxidation," *Applied Physics Express* 2 (2009): 041101.

4. Y. Song, S. Dhar, L. C. Feldman, G. Chung, and J. R. Williams, "Modified Deal Grove Model for the Thermal Oxidation of Silicon Carbide," *Journal of Applied Physics* 95 (2004): 4953–4957.

5. B. K. Daas, M. M. Islam, I. A. Chowdhury, F. Zhao, T. S. Sudarshan, and M. V. S. Chandrashekhar, "Doping Dependence of Thermal Oxidation on n-Type 4H-SiC," *IEEE Transactions on Electron Devices* 58 (2011): 115–121.

6. V. Šimonka, A. Hössinger, J. Weinbub, and S. Selberherr, "Growth Rates of Dry Thermal Oxidation of 4H-Silicon Carbide," *Journal of Applied Physics* 120 (2016): 135705.

7. K. Tachiki, M. Kaneko, and T. Kimoto, "Mobility Improvement of 4H-SiC (0001) MOSFETs by a Three-Step Process of H_2 Etching, SiO_2 Deposition, and Interface Nitridation," *Applied Physics Express* 14 (2021): 031001.

8. M. Cabello, V. Soler, G. Rius, J. Montserrat, J. Rebollo, and P. Godignon, "Advanced Processing for Mobility Improvement in 4H-SiC MOSFETs: A Review," *Materials Science in Semiconductor Processing* 78 (2018): 22–31.

9. P. Fiorenza, F. Giannazzo, A. Frazzetto, and F. Roccaforte, "Influence of the Surface Morphology on the Channel Mobility of Lateral Implanted 4H-SiC(0001) Metal-Oxide-Semiconductor Field-Effect Transistors," *Journal of Applied Physics* 112 (2012): 084501.

10. P. Fiorenza, F. Giannazzo, S. Cascino, M. Saggio, and F. Roccaforte, "Identification of Two Trapping Mechanisms Responsible of the Threshold Voltage Variation in SiO_2/4H-SiC MOSFETs," *Applied Physics Letters* 117 (2020): 103502.

11. Y. Xu, X. Zhu, H. D. Lee, et al., "Atomic State and Characterization of Nitrogen at the SiC/SiO_2 Interface," *Journal of Applied Physics* 115 (2014): 033502.

12. L. K. Swanson, P. Fiorenza, F. Giannazzo, A. Frazzetto, and F. Roccaforte, "Correlating Macroscopic and Nanoscale Electrical Modifications of SiO_2/4H-SiC Interfaces Upon Post-Oxidation-Annealing in N_2O and $POCl_3$," *Applied Physics Letters* 101 (2012): 193501.

13. P. Fiorenza, F. Giannazzo, M. Vivona, A. La Magna, and F. Roccaforte, "SiO_2/4H-SiC Interface Doping During Post-Deposition-Annealing of the Oxide in N_2O or $POCl_3$," *Applied Physics Letters* 103 (2013): 153508.

14. H. Yano, N. Kanafuji, A. Osawa, T. Hatayama, and T. Fuyuki, "Threshold Voltage Instability in 4H-SiC MOSFETs With Phosphorus-Doped and Nitrided Gate Oxides," *IEEE Transactions on Electron Devices* 62 (2015): 324–332.

15. A. J. Lelis, R. Green, D. B. Habersat, and M. El, "Basic Mechanisms of Threshold-Voltage Instability and Implications for Reliability Testing of SiC MOSFETs," *IEEE Transactions on Electron Devices* 62 (2015): 316–323.

16. P. Fiorenza, M. Zignale, M. Camalleri, et al., "Impact of the NO Annealing Duration on the SiO_2/4H–SiC Interface Properties in Lateral MOSFETs: The Energetic Profile of the Near-Interface-Oxide Traps," *Materials Science in Semiconductor Processing* 169 (2024): 107866.

17. T. Kobayashi, K. Tachiki, K. Ito, and T. Kimoto, "Reduction of Interface State Density in SiC (0001) MOS Structures by Low-Oxygen-Partial-Pressure Annealing," *Applied Physics Express* 12 (2019): 031001.

18. Y. Uchida, A. Tamura, and K. Kita, "Enhancement of CMP Removal Rate of SiC by Ion Implantation," *Japanese Journal of Applied Physics* 65 (2026): 088003.

19. H. Yoshida, T. Onaya, A. Tamura, and K. Kita, "Difference in Kinetics Between Thermal Nitridation and Radical Nitridation Processes of 4H-SiC Surface Considering Simultaneous N-Incorporation and N-Desorption Reactions," *Solid-State Electronics* 233 (2026): 109334.

20. T. Kobayashi, T. Okuda, K. Tachiki, K. Ito, Y. Matsushita, and T. Kimoto, "Design and Formation of SiC (0001)/SiO_2 Interfaces via Si Deposition Followed by Low-Temperature Oxidation and High-Temperature Nitridation," *Applied Physics Express* 13 (2020): 091003.

21. K. Tachiki, M. Kaneko, T. Kobayashi, and T. Kimoto, "Formation of High-Quality SiC(0001)/SiO_2 Structures by Excluding Oxidation Process With H_2 Etching Before SiO_2 Deposition and High-Temperature N_2 annealing," *Applied Physics Express* 13 (2020): 121002.

22. M. Z. Alam, I. A. Khan, S. I. Amin, and A. Anam, "Heteroepitaxial β-Ga_2O_3 Trench-Gate MOSFET on 4H-SiC: Trap, Thermal, and Breakdown Optimization," *physica status solidi (a)* 223 (2026): 202500848.

23. T. H. Kil and K. Kita, "Anomalous Band Alignment Change of SiO_2/4H–SiC (0001) and (000–1) MOS Capacitors Induced by NO-POA and its Possible Origin," *Applied Physics Letters* 116 (2020): 122103.

24. T. Yang and K. Kita, "Opportunity to Achieve an Efficient SiC/SiO_2 Interface N passivation by Tuning the Simultaneous Oxidation Modes During the SiC Surface Nitridation in $N_2 + O_2$ Annealing," *Solid-State Electronics* 210 (2023): 108815.

25. T. Yang, T. Onaya, and K. Kita, "Low-Temperature Annealing in O_2 to Annihilate the Fixed Charges in 4H-SiC/SiO_2 Interface Induced by High-N-Density Nitridation Process," *IEEE Electron Device Letters* 45 (2024): 1145–1148.

26. X. Li, A. Ermakov, V. Amarasinghe, E. Garfunkel, T. Gustafsson, and L. C. Feldman, "Oxidation Induced Stress in SiO_2/SiC Structures," *Applied Physics Letters* 110 (2017): 141604.

27. D. Okamoto, M. Sometani, S. Harada, R. Kosugi, Y. Yonezawa, and H. Yano, "Improved Channel Mobility in 4H-SiC MOSFETs by Boron Passivation," *IEEE Electron Device Letters* 35 (2014): 1176–1178.

28. D. J. Lichtenwalner, L. Cheng, S. Dhar, A. Agarwal, and J. W. Palmour, "High Mobility 4H-SiC (0001) Transistors Using Alkali and Alkaline Earth Interface Layers," *Applied Physics Letters* 105 (2014): 182107.

29. J. H. Dycus, W. Xu, D. J. Lichtenwalner, B. Hull, J. W. Palmour, and J. M. LeBeau, "Structure and Chemistry of Passivated SiC/SiO_2 Interfaces," *Applied Physics Letters* 108 (2016): 201607.

30. S. M. Sze and K. K. Ng, *Physics of Semiconductor Devices* (John Wiley & Sons, Inc, 2007).

31. M. Zignale, P. Fiorenza, L. Calcagno, M. Antoniou, F. Giannazzo, and F. Roccaforte, "Calculation of the Whole Interface State Density Profile in SiO_2/SiC Lateral MOSFETs," *Key Engineering Materials* 1055 (2026): 1–6.

32. T. Kobayashi and T. Kimoto, "Carbon Ejection From a SiO_2/SiC(0001) Interface by Annealing in High-Purity Ar," *Applied Physics Letters* 111 (2017): 062101.

33. P. Fiorenza, A. Frazzetto, A. Guarnera, M. Saggio, and F. Roccaforte, "Fowler-Nordheim Tunneling at SiO_2/4H-SiC Interfaces in Metal-Oxide-Semiconductor Field Effect Transistors," *Applied Physics Letters* 105 (2014): 142108.

34. P. Fiorenza, M. Vivona, F. Iucolano, et al., "Temperature-Dependent Fowler-Nordheim Electron Barrier Height in SiO_2/4H-SiC MOS capacitors," *Materials Science in Semiconductor Processing* 78 (2018): 38–42.

35. H. Harima, "Raman Scattering Characterization on SiC," *Microelectronic Engineering* 83 (2006): 126–129.

36. D. Olego, M. Cardona, and P. Vogl, "Pressure Dependence of the Optical Phonons and Transverse Effective Charge in 3C-SiC," *Physical Review B* 25 (1982): 3878–3888.

37. J. Zhang, T. Liang, Y. Lu, et al., "Effect of Hexagonality on the Pressure-Dependent Lattice Dynamics of 4H-SiC," *New Journal of Physics* 24 (2022): 113015.

38. S. Nakashima, T. Kitamura, T. Kato, et al., "Determination of Free Carrier Density in the Low Doping Regime of 4H-SiC by Raman Scattering," *Applied Physics Letters* 93 (2008): 121913.

39. P. Fiorenza, C. Bongiorno, F. Giannazzo, et al., "Interfacial Electrical and Chemical Properties of Deposited SiO_2 Layers in Lateral Implanted 4H-SiC MOSFETs Subjected to Different Nitridations," *Applied Surface Science* 557 (2021): 149752.

40. K. Kakushima, K. Okamoto, M. Adachi, et al., "Origin of Flat Band Voltage Shift in HfO_2 Gate Dielectric With La_2O_3 Insertion," *Solid-State Electronics* 52 (2008): 1280–1284.

41. T.-H. Kil, A. Tamura, S. Shimizu, and K. Kita, "Impacts of Band Alignment Change After Interface Nitridation on the Leakage Current of SiO_2/4H-SiC (0001) and (1100) MOS Capacitors," *Applied Physics Express* 14 (2021): 081005.

42. E. Schilirò, G. Greco, P. Fiorenza, et al., "Comparing Post-Deposition and Post-Metallization Annealing Treatments on Al_2O_3/GaN Capacitors for Different Metal Gates," *AIP Advances* 14 (2024): 105109.

43. N. Ise, T. Akiyama, T. Hatakeyama, K. Shiraishi, and T. Nakayama, "Controlled Synthesis and Se Doping of WTe_2 Nanowires for Enhanced Thermoelectric Performance," *Japanese Journal of Applied Physics* 65 (2026): 03SP06.